J Appl Electrochem (2014) 44:599–606
DOI 10.1007/s10800-014-0658-2

RESEARCH ARTICLE

Synthesis, characterization, and evaluation of unsupported porous NiS submicrometer spheres as a cathode material for lithium batteries

Debajyoti Mondal · Gilles Villemure · Chaojie Song

Received: 25 September 2013 / Accepted: 2 January 2014 / Published online: 28 January 2014

Abstract Synthesis of a nanostructured pure phase nickel sulfide in a single step is a challenge. In this work, a new method for direct synthesis of uniform NiS–SiO_2 submicrospheres was developed by ultrasonic spray pyrolysis. Colloidal silica was used as a sacrificial template to create the porous structure. After silica removal, hollow, porous pure phase NiS nanospheres were obtained. The product was characterized by scanning electron microscopy, energy dispersive X-ray spectroscopy, X-ray diffraction, transmission electron microscopy, and N_2 adsorption/desorption isotherm. The results confirmed the formation of single phase millerite NiS porous nanospheres with a high surface area of 312 $m^2\ g^{-1}$. The NiS spheres were tested as cathode for lithium batteries. A discharge capacity of 340 mAh g^{-1} with good capacity retention during multiple cycles was obtained.

Keywords Nickel sulfide · Ultrasonic spray pyrolysis · Lithium battery · Electrode materials · Galvanostatic testing

1 Introduction

Transition metal semiconductor chalcogenides have attracted intensive interest because of their versatile optical [1], magnetic [2], and catalytic [3] properties. Important transition metal sulfides include cadmium sulfide [4], zinc sulfide [5, 6], manganese sulfide [7], silver sulfide [7], iron sulfide [8], nickel sulfide [9, 10], and many phases of copper sulfide [11], which have a wide range of applications ranging from cathode materials in rechargeable lithium batteries [11], IR detectors [12, 13], transformation toughener [14], paramagnetic–antiferromagnetic phase-changing materials [15], catalysts for photogalvanic cells [14], for the degradation of organic dyes [16] or for hydrodesulfurization of heavy oil [17, 18]. Nickel sulfides were first reported by Kullerud and Yund [19] in 1962, followed by others [20–23]. Nickel sulfides have attracted interest because of their wide variety of applications due to their various phases such as hydrotreating catalysts [17]. The compositions and phases of nickel sulfides reported in the literature include NiS, α-$Ni_{3+x}S_2$, β-Ni_3S_2, Ni_7S_6, Ni_9S_8, Ni_3S_4, and NiS_2. NiS comes into two main phases, a hexagonal NiS (h-NiS) [23] and rhombohedral NiS (r-NiS) [24].

As environmental regulations on fossil fuels such as gasoline and diesel become more stringent, electric vehicles (EVs), hybrid electric vehicles (HEVs) with controlled greenhouse gas emission will be the next generation mainstream transportation vehicles. Lithium batteries are considered to be the most promising power source for EVs and HEVs, due to their high operating voltage and high energy density. Since the introduction of lithium batteries by Sony Energetic Inc. [25], enormous research effort has been made in this area. For EVs and HEVs applications, lithium batteries with higher charge and discharge capacities, better cyclic stability, and longer lifetime are needed. Cathode materials are the limiting factor hindering current batteries' application in EVs and HEVs. Metal sulfides are one type of new active cathode materials for rechargeable lithium batteries [12, 26–33]. These sulfides have high

D. Mondal · G. Villemure (✉)
Department of Chemistry, University of New Brunswick, Fredericton, NB, Canada
e-mail: gvd@unb.ca

D. Mondal · C. Song (✉)
Energy, Mining and Environment, NRC, 4250 Wesbrook Mall, Vancouver, BC V6T 1W5, Canada
e-mail: chaojie.song@nrc.gc.ca

theoretical capacity. NiS has a theoretical capacity of 590 mAh g^{-1}, higher than the widely used $LiCoO_2$ (280 mAh g^{-1}) [34] and $LiFePO_4$ (170 mAh g^{-1}) [35]. It also has high electronic conduction and high lithium activity [36, 37].

Several methods have been reported for NiS preparation. The simplest one is direct stoichiometric combination of constituent elements [38]. Kosmac et al. [39] synthesized NiS by mechanical alloying of nickel and sulfur powder. NiS could also be synthesized by homogeneous sulfide precipitation method [17, 18]. Other techniques to prepare NiS include mechanochemical [40], solvothermal [41], hydrothermal [42], sparks plasma-sintering [43], high-boiling point solvent [44], polyol [37], etc. Recently nanostructured NiS was prepared by a variety of new methods. Hu et al. [45] used gamma irradiation to prepare NiS microspheres. Korgel et al. [46] synthesized NiS nanorods and triangular nanoprisms from molecular precursors by solventless thermolysis. Urchin-like NiS was synthesized by a solvothermal method [47]. Nanostructured NiS was also synthesized by a soft solution process [9], sonochemical technique [48], hydrogel method [49], microemulsion method [50], thermal decomposition process [51], etc.

Ultrasonic spray pyrolysis (USP), an aerosol synthetic technique, can produce nanostructured products in a single step. A variety of nanostructured materials have been synthesized using this method. Using a sacrificial template may create a porous structure in the product [52, 53]. Hollow spherical products have advantages over solid spheres and other nanostructures due to their higher specific surface area and better permeability.

The advantages of high theoretical lithium storage capacity of NiS, unique advantages of porous structure within nanospheres, and the uniqueness of USP technology motivated us to prepare porous NiS nanospheres using USP method for lithium battery application. In this work, we prepared well-defined crystalline porous NiS spheres with high surface area (312 m^2 g^{-1}). To the best of our knowledge, this is the first report on the synthesis of porous submicrometer-sized spheres of pure millerite NiS using the USP method and the first report on NiS with such a high surface area. The product was tested as a cathode material for rechargeable lithium batteries and showed promising results with reasonable discharge capacity and a significantly improved cycle life.

2 Experimental

2.1 Chemical and materials

All reagents were of analytical grade and used as received. $NiCl_2{\cdot}6H_2O$ and $Na_2S_2O_3{\cdot}5H_2O$ were obtained from Sigma-Aldrich, and colloidal silica (35 wt% of silica suspended in water, particle diameter ca 3 nm) was obtained from AzkoNobel/Eka.

2.2 Synthesis of porous NiS submicrospheres

The USP procedure for the synthesis of nanomaterials was reported elsewhere [54]. A solution containing $NiCl_2{\cdot}6H_2O$, $Na_2S_2O_3{\cdot}5H_2O$, and colloidal silica was prepared according to a procedure reported in our previous paper [55]. The solution was loaded to a USP ultrasonic cell, after which the system was purged with Ar for 30 min. Then, the solution was nebulized with an ultrasonic atomizer (2.4 MHz, Sonaer Inc., Farmingdale, NY). Ar (flow rate: 5 L min^{-1}) was used to carry the aerosol mist through a tube furnace at 450 °C. The product was collected, filtered, washed with DI water, and dried at room temperature. The silica template was removed by etching in a 5 % HF solution. The final product was centrifuged and washed several times with ethanol and deionized water followed by drying under vacuum at 70 °C for 12 h.

2.3 Physical characterization

Scanning electron microscopy (SEM), transmission electron microscopy (TEM), powder X-ray diffraction (XRD), energy dispersive X-ray spectroscopy (EDX), and N_2-sorptometry were used to characterize the product. SEM images were obtained using a FEI Dual Beam Strata 235 scanning electron microscope operating at 5 kV. The transmission electron micrographs were taken on a JEOL 2011 scanning transmission electron microscope operating at 200 keV. The micrographs were recorded digitally using a CCD camera (Gatan 4k×4k Ultrascan). TEM/EDX elemental analysis of the product was done on the same instrument using an EDAX (Genesis) energy dispersive X-ray system. The XRD patterns were obtained on a Bruker D8 X-ray diffractometer using Cu Kα radiation at 40 kV and 20 mA and a scanning rate of 0.04 2θ s^{-1}. Nitrogen adsorption/desorption isotherm was recorded on a Quantachrome Autosorb-1 instrument. The powder was out-gassed at 70 °C for 8 h before the measurements.

2.4 Electrochemical tests

The electrode was prepared as follows: 70 wt% porous spherical NiS was mixed with 20 wt% acetylene black and 10 wt% poly(vinylidene fluoride) (PVDF). *N*-Methyl-2-pyrrolidinone was added as a dispersant to form a paste, which was spread onto aluminum foil substrates, and kept at vacuum for drying. The NiS-loaded aluminum foils were cut into 15-mm diameter disks by a MTI precision disk cutter MSK-T-06, which was used as the cathode. All the other components of the CR2032 coin cell including

stainless steel spacer, spring, and lithium battery separator film were from MTI Corporation and assembled in an argon-filled glove box using a house designed and fabricated coin cell crimper CR100. A lithium metal disk was used as the anode. The electrolyte was composed of 1 mol L^{-1} $LiPF_6$ dissolved in ethylene carbonate/diethyl carbonate with the ratio of 1:1. The charge–discharge cycles of the cells were performed using a Keithley 2400 source meter in a potential range of 1.0–3.0 V at a current density of 50 mA g^{-1}.

3 Results and discussion

3.1 Morphology and structure of nickel sulfide submicrospheres

Scanning electron microscopy and TEM images of the NiS–SiO_2 composite are shown in Fig. 1a, b, respectively. It is evident that the product consists of submicrometer-sized spheres (500 ± 200 nm). EDX analysis of the composite confirmed the presence of nickel and sulfur, with a molar ratio of 1:1 and Si from the SiO_2 template (Fig. 2a), which is consistent with NiS–SiO_2 composite. Figure 2b is the electron diffraction pattern (ED) of the product. A continuous ring with fine spots in ED confirms a polycrystalline material composed of nano crystallites.

Figure 3 shows the XRD pattern of the synthesized product. It shows reflections from 101, 300, 021, 211, 131, 410, 401, 321, 330, 012, and 600 planes of millerite NiS at two theta degree of 32.3, 35.7, 37.5, 40.5, 48.9, 50.3, 52.7, 56.3, 57.6, 59.6, and 67.5, respectively. All these diffraction peaks are assigned to a pure millerite NiS and are consistent with the reported data for millerite, nickel sulfide (NiS, JCPDS Card No. 12-0041, space group R3 m, cell parameters $a = 9.62$ Å, $c = 3.16$ Å). All other peaks in the diffraction pattern are attributed to the SiO_2 template, present in the synthesized NiS–SiO_2 composite. The good crystallinity of the product is demonstrated by the sharp diffraction peaks in the XRD pattern.

To remove the silica template, the NiS–SiO_2 composite material was subjected to HF etching. EDX analysis of the product after HF treatment showed the presence of nickel, sulfur, and trace amounts of oxygen (Fig. 4) indicating that SiO_2 was successfully removed. A TEM micrograph of the product after HF treatment is shown in Fig. 5a. It is evident that the spherical morphology of the composite was not damaged during the SiO_2 removal process. Figure 5b shows the magnified image of a similar spherical structure. It reveals that the spheres are composed of nanocrystalline NiS particles with average particle size of 10–15 nm with pores on the surface. Figure 5c shows the XRD pattern of the NiS spheres after SiO_2 removal. Diffraction peaks

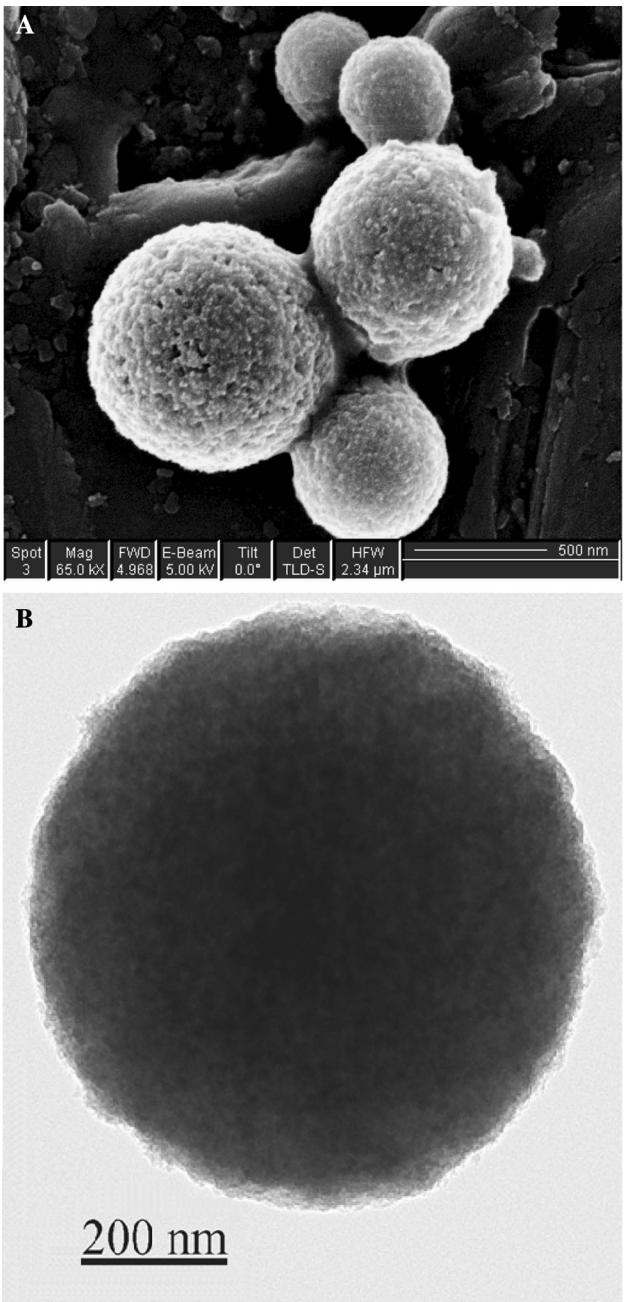

Fig. 1 **a** SEM image of the spherical NiS–SiO_2 composite. **b** TEM image of the spherical NiS–SiO_2 composite

related to SiO_2 were gone, and no phase change was observed with NiS after SiO_2 removal.

Figure 6 shows N_2 adsorption/desorption isotherms for NiS–SiO_2 composite (a) and SiO_2-free spherical NiS (b) The isotherm for silica-free nanostructure indicates the presence of micro and macroporosity in the product. The BET surface area of the silica-free NiS is 312 m^2 g^{-1}, a significant increase from 35 m^2 g^{-1} for the NiS–SiO_2 composite. This is not unexpected as removal of silica

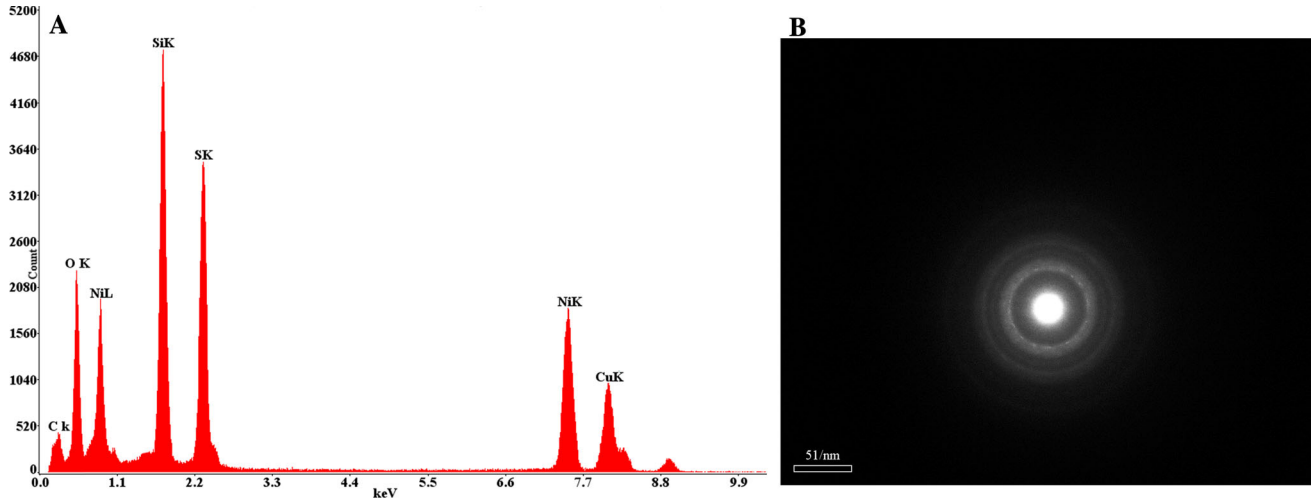

Fig. 2 **a** TEM–EDX spectra of as-prepared NiS–SiO_2 composite. **b** Electron diffraction pattern of the nanostructured NiS

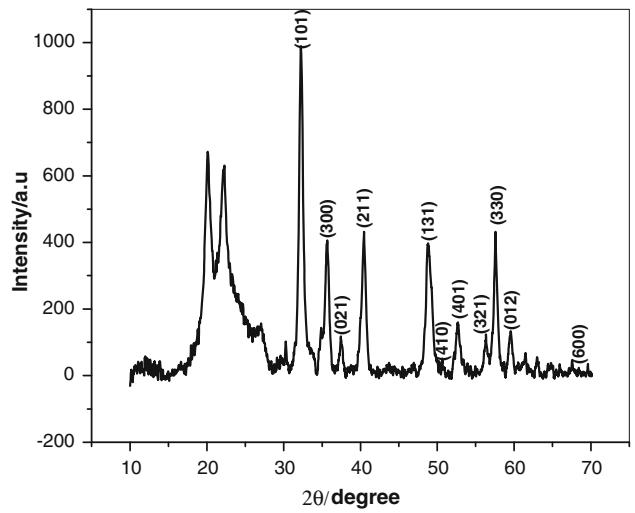

Fig. 3 Powder XRD of the as-synthesized NiS–SiO_2

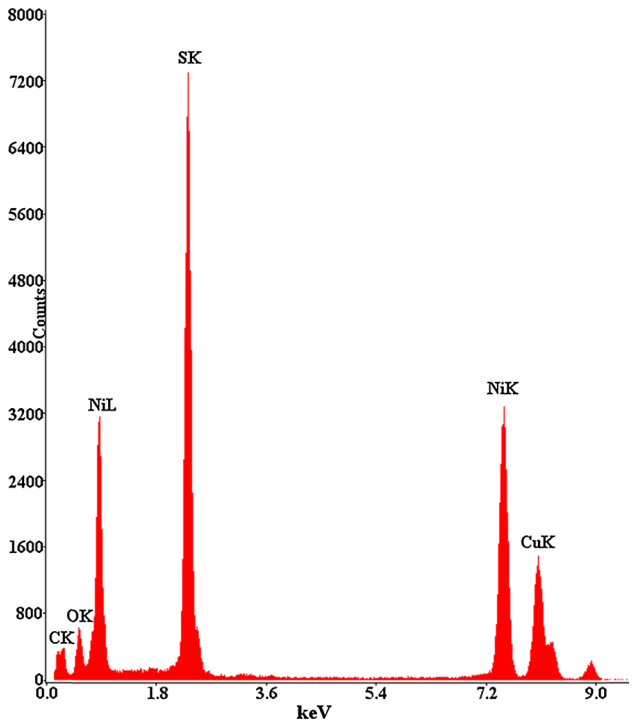

Fig. 4 TEM–EDX spectra of hollow spherical NiS submicrosphere after HF treatment

creates numerous pores in the spheres, increasing the surface area.

In summary, the reaction mixture containing $NiCl_2{\cdot}6H_2O$, $Na_2S_2O_3{\cdot}5H_2O$, and colloidal silica produced millerite NiS via USP at 450 °C. Note that we found that the composition and phase of the produced nickel sulfides could be precisely controlled just by simply changing the furnace temperature. In a previous report, we synthesized pure phase cubic nickel disulfide using the same reactant mixture but at a lower furnace temperature of 300 °C [55]. Thus, USP is a convenient method to produce pure nickel sulfides of different compositions and phases.

3.2 Electrochemical performances

The nickel sulfide electrode was incorporated in a CR2032 coin cell as cathode, and their electrochemical properties were tested using galvanostatic charge/discharge cycling. Figure 7 shows the first discharge curve. The discharge curve begins with a steep fall followed by two plateaus, ranging from 1.7 to 1.81 V and 1.3 to 1.4 V. These two plateaus are indicative of the two-step electrochemical reactions between NiS and Li during the discharging process. As previously reported [12], the first plateau was attributed to the reaction of NiS with Li to produce Ni_3S_2 (Eq. 1), which further reacted with Li to form nickel

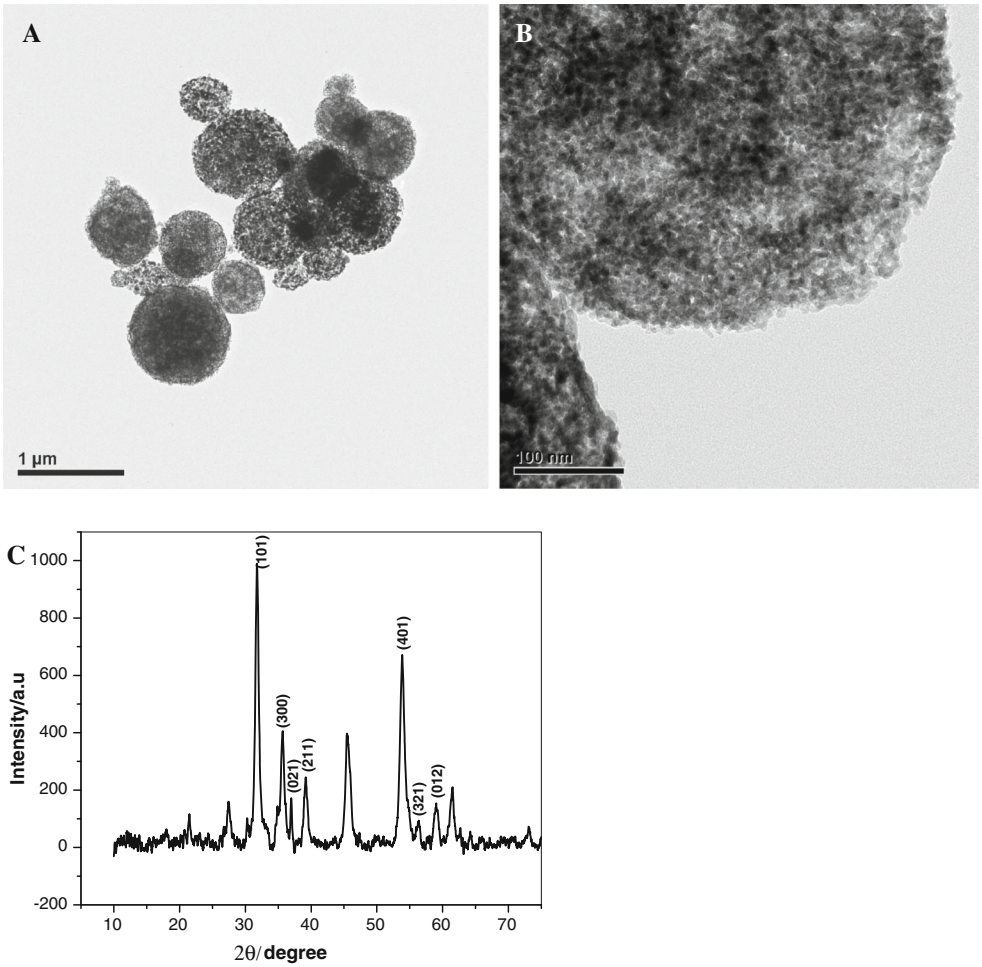

Fig. 5 **a** TEM image of the spherical hollow NiS. **b** TEM image of the spherical hollow NiS showing individual NiS particles which are 10–15 nm in size. **c** XRD pattern of the NiS spheres after SiO_2 removal

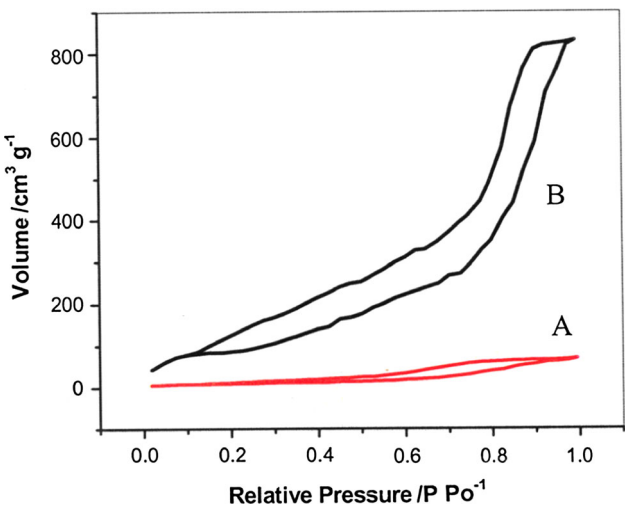

Fig. 6 N_2 adsorption/desorption isotherms for *a* NiS–SiO_2 composite and *b* SiO_2-free hollow NiS submicrosphere

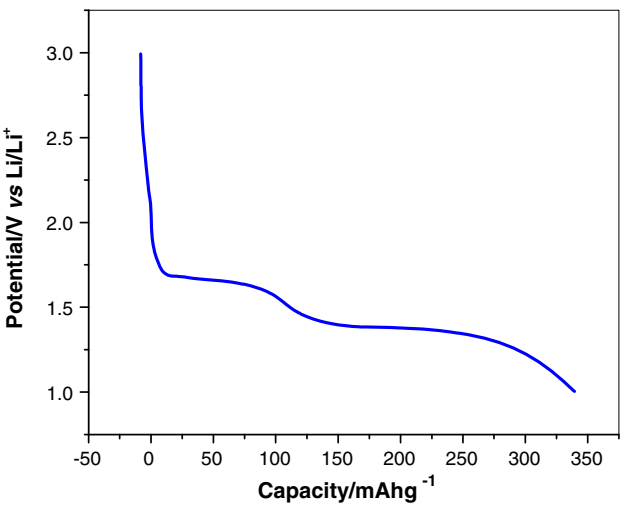

Fig. 7 First discharge curve of the porous spherical NiS electrode

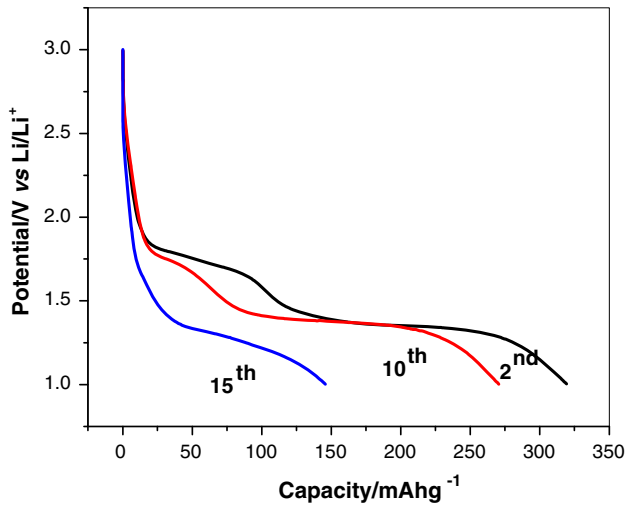

Fig. 8 Comparison of the 2nd, 10th, and 15th discharge curves of the porous spherical NiS electrode

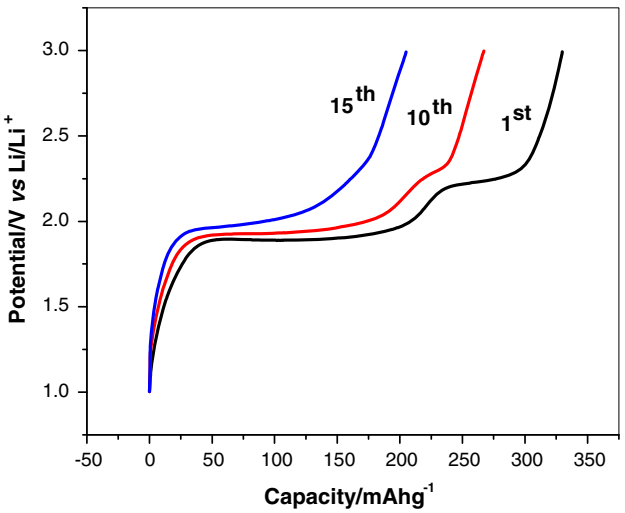

Fig. 9 Comparison of the 1st, 10th, and 15th discharge curves of the porous spherical NiS electrode

(Eq. 2), resulting in the second plateau. In both reactions Li_2S is produced. The overall charging–discharging reaction is represented by Eq. 3 [12].

$$3NiS + 2Li \rightleftharpoons Ni_3S_2 + Li_2S \quad (1)$$

$$Ni_3S_2 + 4Li \rightleftharpoons 3Ni + 2Li_2S \quad (2)$$

$$NiS + 2Li \rightleftharpoons Ni + Li_2S \quad (3)$$

The first discharge capacity of the material was found to be 340 mAh g^{-1}. This value is lower than the theoretical capacity of NiS (590 mAh g^{-1}) and the capacity of comparable materials [56]. However, the porous NiS nanospheres showed potentially better capacity retention during multiple charging–discharging cycles.

Figure 8 shows the comparison between the 2nd, 10th, and 15th discharge curves. The first discharge plateau at 1.7–1.8 V shrinks as cycling continues. It eventually disappears at the 15th cycle. The discharge capacity of the second cycle was 320 mAh g^{-1}, a capacity retention of over 94 %, while after the 15th cycle the discharge capacity was 146 mAh g^{-1}, a capacity retention of 43 %, much higher than comparable NiS cathode materials for lithium batteries [56]. This indicates that the NiS nanospheres have good cycling stability. Wang et al. [56] reported a discharge capacity of 588 mAh g^{-1} for NiS hollow microspheres in the first cycle. However, it was reduced to 206 mAh g^{-1} at 5th cycle and 84 mAh g^{-1} at the end of 20th cycle, a capacity retention of only 14 %.

Typically, a NiS-based cathode of a lithium battery rapidly loses its discharging capacity with the number of cycles starting at the 2nd charging/discharging cycle [40, 56]. Such capacity decay is attributed to the formation of lithium polysulfide during the discharge reaction. Solubility of lithium polysulfide in the electrolyte coupled with its low ionic and electronic conductivity accounts for the capacity decrease. Capacity loss of the cell can also be related to the contact loss between the NiS active material and the current collector due to the volume change of the active materials during Li^+ insertion/extraction. However, in the case of hollow porous spheres of NiS, such loss in discharge capacity is not as rapid as previously reported for NiS cathode materials [56]. It may be attributed to the very high surface area of the porous spherical structure of the NiS electrode. Such structure could enhance the amount of lithium intercalated in the material. It could also improve the effective contact area between the electrode and the electrolyte, dissipating the accumulation of Li^+ ions hence accommodating the strain of the Li^+ insertion/extraction, and enhancing mobility.

Figure 9 compares the 1st, 10th, and 15th charge curves. The first charge curve shows three sloping potential regions ranging from 1.0 to 1.88 V, 1.93 to 2.21 V, and 2.25 to 3 V with two plateau regions at 1.9 and 2.2 V. Again, these plateaus shrink with continuous cycling and eventually disappear after certain cycles. The 10th charge curve exhibits two sloping potential regions ranging from 1.0 to 1.91 V and 1.95 to 3 V with a plateau region from 1.91 to 1.95 V and a hint of plateau near 2.3 V. The 15th charge curve shows two sloping potential regions ranging from 1.0 to 1.95 V and 1.98 to 3 V without a plateau region. These curves correspond to the regeneration of nickel sulfides during the charging process. Overall, the coulombic efficiency for the first charging/discharging cycle is found to be 98 %, and it is still more than 95 % for the 15th charging/discharging cycle which is indicative of an efficient charging/discharging process for the coin cell.

4 Conclusions

Nanostructured hollow NiS submicrometer spheres were successfully synthesized using the USP method. It was found that phase and composition of the produced nickel sulfide can precisely be controlled by this procedure. Additionally, this synthesis procedure provides a single step, continuous and scalable route to make millerite NiS–SiO_2 composite and further template-free porous millerite NiS with high surface area. The synthesized material has uniform Ni and S distribution and a uniform sphere size of 500 ± 200 nm. The unique porous spherical structure of NiS shows better Li storage capacity during charge–discharge cycles. As a result, such a material can retain more than 40 % of its initial capacity even after the 15th charge–discharge cycle, which makes it a promising candidate for lithium batteries.

Acknowledgments The authors would like to thank the Energy, Mining and Environment, National Research Council of Canada, and the University of New Brunswick for their financial support.

References

1. Gaponenko SV (1998) Optical properties of semiconductor nanocrystals. Cambridge University Press, Cambridge
2. Leslie-Pelecy DL, Rieke RD (1996) Magnetic properties of nanostructured materials. Chem Mater 8:1770–1783
3. Ying JY (2006) Design and synthesis of nanostructured catalysts. Chem Eng Sci 61:1540–1548
4. Murray CB, Norris DJ, Bawendi MG (1993) Synthesis and characterization of nearly monodisperse CdE (E = sulfur, selenium, tellurium) semiconductor nanocrystallites. J Am Chem Soc 115:8706–8715
5. Zhong X, Liu S, Zhang Z, Li L, Wei Z, Knoll W (2004) Synthesis of high-quality CdS, ZnS, and $Zn_xCd_{1-x}S$ nanocrystals using metal salts and elemental sulfur. J Mater Chem 14:2790–2794
6. Quan Z, Wang Z, Yang P, Lin J, Fang J (2007) Synthesis and characterization of high-quality ZnS, ZnS:Mn^{2+}, and ZnS:Mn^{2+}/ZnS (core/shell) luminescent nanocrystals. Inorg Chem 46: 1354–1360
7. Wang D, Zheng W, Hao C, Peng Q, Li Y (2009) A synthetic method for transition-metal chalcogenide nanocrystals. Chem Eur J 15:1870–1875
8. Chen X, Zhang X, Wan J, Wang Z, Qian Y (2005) Selective fabrication of metastable greigite (Fe_3S_4) nanocrystallites and its magnetic properties through a simple solution-based route. Chem Phys Lett 403:396–399
9. Yu S, Yoshimura M (2002) Fabrication of powders and thin films of various nickel sulfides by soft solution-processing routes. Adv Funct Mater 12:277–285
10. Yang S, Yao H, Gao M, Yu S (2009) Monodisperse cubic pyrite NiS2 dodecahedrons and microspheres synthesized by a solvothermal process in a mixed solvent: thermal stability and magnetic properties. Cryst Eng Comm 11:1383–1390
11. Sigman MBJ, Ghezelbash A, Hanrath AT, Saunders AE, Lee F, Korgel BA (2003) Solventless synthesis of monodisperse Cu_2S nanorods, nanodisks, and nanoplatelets. J Am Chem Soc 125:16050–16057
12. Han S, Kim KW, Ahn HJ, Lee JY (2003) Charge–discharge mechanism of mechanically alloyed NiS used as a cathode in rechargeable lithium batteries. J Alloys Compd 361:247–251
13. Atay F, Ose SK, Bilgin V, Akyuz I (2003) Electrical, optical, structural and morphological properties of NiS films. Turk J Phys 27:285–292
14. Kriven WM (1990) Martensitic toughening of ceramics. Mater Sci Eng A 127:249–255
15. Wong E, Sheeleigh CW, Rananvare SB (1992) Structural studies of catalytic nanoparticles. Proceedings of the sixth annual conference on fossil energy materials, Oak Ridge, NETL Publications
16. Kapinus EI, Viktorova TI, Khalyavka TA (2006) Photocatalytic activity of nanoparticles of metal sulfides in the degradation of organic dyes. Theor Exp Chem 42:282–286
17. Olivas A, Cruz-Reyes J, Avalos M, Petranovskii V, Fuentes S (1999) Influence of preparation conditions on formation of crystalline phases of nickel sulfide. Mater Lett 38:141–144
18. Olivas J, Cruz-Reyes J, Avalos M, Petranovskii V, Fu-entes S (1998) Synthesis and characterization of nickel sulfide catalysts. J Vac Sci Technol A 16:3515–3520
19. Kullerud GR, Yund A (1962) The Ni–S system and related minerals. J Petrol 3:126–175
20. Rao CNR, Pisharody PR (1976) Transition metal sulfides. Prog Solid State Chem 10:207–270
21. Stolen S, Fjellvag F, Gronvold F, Seim H, Westrum E (1994) Phase stability and structural properties of $Ni_{7\pm\delta}S_6$ and Ni9S8 Heat capacity and thermodynamic properties of Ni_7S_6 at temperatures from 5 to 970 K and of Ni_9S_8 from 5 to 673 K. J Chem Thermodyn 26:987–1000
22. Jeong YU, Manthiram A (2001) Synthesis of nickel sulfides in aqueous solutions using sodium dithionite. Inorg Chem 40:73–77
23. Wang L, Zhu Y, Li H, Li Q, Qian Y (2010) Hydrothermal synthesis of NiS nanobelts and NiS_2 microspheres constructed of cuboids architectures. J Solid State Chem 183:223–227
24. Zhang X, Wang C, Xie Y, Qian Y (1999) Preparation and characterization of nanocrystalline nickel monosulfide (h) via the ethanol-thermal reducing process. Mater Res Bull 34:1967–1972
25. Nagaura T, Tozawa K (1990) Prog batteries sol cells, vol 9. JEC Press Inc., Brunswick, p 209
26. Wang G, Bewlay S, Yao J, Liu H, Dou S (2004) Tungsten disulfide nanotubes for lithium storage. Electrochem Solid State Lett 7:A321–A323
27. Zhu X, Wen Z, Gu Z, Huang S (2006) Room-temperature mechanosynthesis of Ni_3S_2 as cathode material for rechargeable lithium polymer batteries. J Electrochem Soc 153:A504–A507
28. Jasinski R, Burrows B (1969) Cathodic discharge of nickel sulfide in a propylene carbonate–$LiClO_4$ electrolyte. J Electrochem Soc 116:422–424
29. Jacobson AJ, Chianelli RR, Rich SM, Whittingham MS (1979) Amorphous molybdenum trisulfide: a new lithium battery cathode. Mater Res Bull 14:1437–1448
30. Chen J, Tao Z, Li S (2003) Lithium intercalation in open-ended TiS_2 nanotubes. Angew Chem Int Ed 42:2147–2151
31. Dusheiko VA, Lipkin MS (1995) Synthesis of sulfide cathodic materials and study of their physicochemical properties and electrochemical activity. J Power Sources 54:264–267
32. Gabano JP, De'chenaux V, Gerbier G, Jammet J (1972) D-size lithium cupric sulfide cells. J Electrochem Soc 19:459–461
33. Jasinski RJ, Gaines LH Lithium batteries having a cathode composition comprising a mixture of nickel sulfide and aluminum. US Patent 3749607
34. Mizushima K, Jones PC, Wiseman PJ, Goodenough JB (1980) Li_xCoO_2 ($0 < x < -1$): a new cathode material for batteries of high energy density. Mat Res Bull 15:783–789
35. http://en.wikipedia.org/wiki/Lithium_iron_phosphate Accessed 23 Jan 2013

36. Lai CH, Huang KW, Cheng JH, Lee CY, Lee WF, Huang C, Hwang BJ, Chen LJ (2009) Oriented growth of large-scale nickel sulfide nanowire arrays via a general solution route for lithium-ion battery cathode applications. J Mater Chem 19:7277–7283
37. Wang J, Chew SY, Wexler D, Wang G, Ng SH, Zhong S, Liu H (2007) Nanostructured nickel sulfide synthesized via a polyol route as a cathode material for the rechargeable lithium battery. Electrochem Commun 9:1877–1880
38. Pfeiffer I (1958) Untersuchungen uber den angriff von schwefel auf nickel und nickellegierungen. Z Metallkd 49:267–275
39. Kosmac T, Maurice D, Courtney TH (1993) Synthesis of nickel sulfides by mechanical alloying. J Am Ceram Soc 76:2345–2352
40. Nishio Y, Kitaura H, Hayashi A, Tatsumisago M (2009) All-solid-state lithium secondary batteries using nanocomposites of NiS electrode/Li_2S–P_2S_5 electrolyte prepared via mechano-chemical reaction. J Power Sources 189:629–632
41. Wang J, Chou SL, Chew SY, Sun JZ, Forsyth M, MacFarlane DR, Liu H (2008) Nickel sulfide cathode in combination with an ionic liquid-based electrolyte for rechargeable lithium batteries. Solid State Ion 179:2379–2382
42. Idris NH, Rahmana MM, Lei S, Choua S, Wang J, Wexlerc D, Liua H (2011) Rapid synthesis of binary α-NiS–β-NiS by microwave autoclave for rechargeable lithium batteries. Electrochim Acta 58:456–462
43. Takeuchi T, Sakaebe H, Kageyama H, Handa K, Sakai T, Tatsumi K (2009) Modification of nickel sulfide by surface coating with TiO_2 and ZrO_2 for improvement of cycle capability. J Electrochem Soc 156:A958–A966
44. Aso K, Kitaura H, Hayashi A, Tatsumisago M (2011) Synthesis of nanosized nickel sulfide in high-boiling solvent for all-solid-state lithium secondary batteries. J Mater Chem 21:2987–2990
45. Hu Y, Chen J, Chen W, Lin X, Li X (2003) Synthesis of novel nickel sulfide submicrometer hollow spheres. Adv Mater 15:726–729
46. Ghezelbash A, Sigman MB, Korgel BA (2004) Solventless synthesis of nickel sulfide nanorods and triangular nanoprisms. Nano Lett 4:537–542
47. Zhang W, Xu L, Tang K, Li F, Qian Y (2005) Solvothermal synthesis of NiS 3D nanostructures. Eur J Inorg Chem 4:653–656
48. Wang H, Zhang J, Zhao X, Xu S, Zhu J (2002) Preparation of copper monosulfide and nickel monosulfide nanoparticles by sonochemical method. Mater Lett 55:253–258
49. Bao C, Lu R, Xue P, Jin M, Tan C, Liu G, Zhao Y (2006) Generation of CdS nano-necklaces and NiS nanotubes templated by sugar-appended hydrogel. J Nanosci Nanotechnol 6:807–812
50. Khiew PS, Huang N, Radiman S, MdS Ahmad (2004) Synthesis of NiS nanoparticles using a sugar-ester non ionic water-in-oil microemulsion. Mater Lett 58:762–767
51. Ghezelbash A, Korgel BA (2005) Nickel sulfide and copper sulfide nanocrystal synthesis and polymorphism. Langmuir 21:9451–9456
52. Skrabalak SE, Suslick KS (2005) Porous MoS_2 synthesized by ultrasonic spray pyrolysis. J Am Chem Soc 127:9990–9991
53. Zhu J, Zhang D, Bian Z, Li G, Huo Y, Lu Y, Li H (2009) Aerosol-spraying synthesis of SiO_2–TiO_2 nanocomposites and conversion to porous TiO_2 and single-crystalline $TiOF_2$. Chem Commun 36:5394–5396
54. Yao S, Song C, Nan F, Botton GA, Chen J, Fairbridge C, Hui R, Zhang J (2012) Synthesis of hierarchical structured porous MoS_2–SiO_2 microspheres by ultrasonic spray pyrolysis. Can J Chem Eng 90:330–335
55. Mondal D, Villemure G, Li G, Song C, Zhang J, Hui R, Chen J, Fairbridge C (2013) Synthesis, characterization and evaluation of unsupported porous NiS_2 sub-micrometer spheres as a potential hydrodesulfurization catalyst. Appl Catal A Gen 450:230–236
56. Wang Y, Zhu Q, Taob L, Sua X (2011) Controlled-synthesis of NiS hierarchical hollow microspheres with different building blocks and their application in lithium batteries. J Mater Chem 21:9248–9254